Energy Proceedings
Vol 31, 2023
ISSN 2004-2965

Combustion Performance Analysis of X-type Rotary Engine with Premixing of Hydrogen and Gasoline

Qi Geng [1], Zhenghao Yang [1], Yang Du [2], Guangyu He [1]*

1 Science and Technology on Plasma Dynamics Laboratory, Air Force Engineering University

2 School of Mechanical Engineering, Xi'an Jiaotong University

ABSTRACT

This paper mainly investigates the effect of the premixing of hydrogen and gasoline (PHG) on the flow and combustion characteristics of the X-type rotary engine (XRE). The three-dimensional numerical simulation model is firstly established based on CFD software. Then, the flow fields and combustion performances of XRE under 1%, 3% and 5% energy fractions of hydrogen-blended (EFHB) are compared and analyzed. The results show that the in-cylinder mean turbulent kinetic energy (TKE) and vorticity present three peaks at the beginning, middle and end stage of the intake process, respectively. Meanwhile, the peak in the middle stage is the largest and steepest, indicating that the in-cylinder flow field is fully mixing air and fuel at this stage. The PHG can produce more OH, O and H radicals, and accelerate the combustion process. Furthermore, the PHG can increase the combustion temperature. In particular, the peak of the in-cylinder mean temperature is increased by 6.4% when the EFHB is 5%. The hydrogen can broaden the combustion area to both sides of the combustion chamber, and help to solve the problem of incomplete combustion in the slit of the combustion chamber of XRE.

Keywords: X-type rotary engine; premixing of hydrogen and gasoline; flow field; combustion performance;

NONMENCLATURE

Abbreviations	
CFD	Computational Fluid Dynamics
PHG	Premixing of hydrogen and gasoline
XRE	X-type rotary engine
WRE	Wankel rotary engine
EFHB	energy fraction of hydrogen-blended
HB	hydrogen-blended
TKE	turbulent kinetic energy
BTDC	before top dad center
ATDC	after top dad center
Symbols	
°CA	engine crankshaft angle

1. INTRODUCTION

XRE is a new type of rotary engine with novel structural features of ellipse rotor profile and triangular cylinder profile [1], which could overcome the problems of high fuel consumption, sealing and lubrication in traditional Wankel rotary engine (WRE) [2-3]. The United States Liquid piston company has developed three XRE [4-7]: 70cc displacement XMv3 type, 130cc displacement X1 type, 750cc displacement X4 type. However, the company researches just focused on the theoretical analysis of thermodynamic performance of XRE using fossil fuels such as gasoline or kerosene. The studies on the internal flow fields and combustion performances of XRE using hydrogen-blended (HB) fuel are few.

As a clean, efficient and green energy source, hydrogen has the advantages of high flame speed, short quenching distance, fast diffusion rate, wide combustion limit and low calorific value [8-9], which is suitable for combustion in a high-speed WRE [10-11]. To further improve the performance of XRE, HB can be one of the effective measures to improve combustion performance. However, their studies focused on the effect of HB on WRE with traditional structure, while the effect of HB on XRE with different structures has not been studied.

Therefore, a CFD model was developed to investigate the effect of PHG on XRE in this paper.

2. SIMULATION MODEL BUILDING AND VALIDATION

2.1 Physical model building

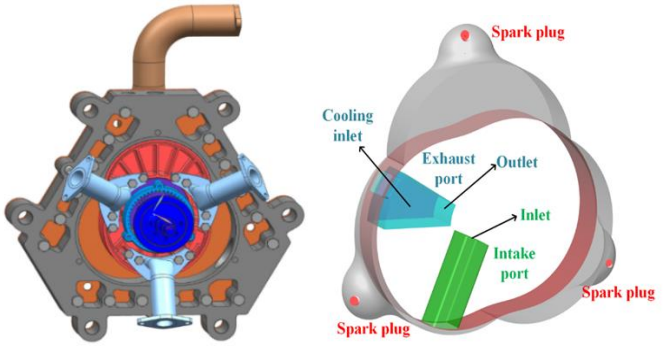

(a) (b)

Fig. 1. Geometry structure (a) and CFD physical model (b) of XRE

The basic 3D geometry of XRE is shown in Fig.1. (a). The gas exchange process of this engine is as follows: the combustible mixture flows into the cylinder from the hollow eccentric shaft to the intake duct on the rotor, and the combustible exhaust gas is discharged from the engine through another engine end cover [5]. The CFD model established in this paper is based on XMv3 engine, whose basic 3D geometric parameters are shown in Table 1. The CFD physical model established according to the parameters is shown in Fig.1. (b).

Table 1 Main structural parameters of XMv3 engine [5]

Project	*Value*
Generating radius/mm	41
Eccentricity/mm	6
Cylinder thick/mm	18.5
Offset/mm	0.7
Geometry compression ratio	11:1
One chamber displacement/cc	23
Cooling method	Water cooled
Ignition source	Spark plug
Top dead center angle/°CA	360
Intake value closing/°CA	585
Exhaust value opening /°CA	161

2.2 Determination of boundary conditions

The in-cylinder flow, flame propagation process and distribution characteristics of the XRE with PHG are studied under the operating conditions in Table 2. The HB method is to mix gasoline and hydrogen at the intake port. Simultaneously, the HB ratio is is to change the energy percentage of hydrogen while keeping the total equivalence ratio of gasoline-hydrogen fuel unchanged.

Table 2 Calculated initial conditions [5]

Calculated parameters	*Value*
Engine speed/RPM	9000
Intake pressure/bar	1.03
Spark advance angle/°CA	30
Cooling gas flow to housing/Kg*sec-1	171
Fuel	gasoline
Equivalent ratio	1.12
EFHB	1%、3%、5%

In terms of simulation model selection, the RNG model is used as the turbulence model [12], the Han-Reitz model is used as the wall heat transfer model, and the SAGE combustion model is used as the combustion model. For gasoline-hydrogen fuel, the isooctane IC8H18 skeleton reaction mechanism proposed by Liu et al. [13] is used, which also contains a detailed hydrogen oxidation mechanism. Thus, it can be used for numerical simulation studies of gasoline-hydrogen combustion characteristics. The ignition model adopts the way of adding ignition energy that is 20 mJ. Three 0.5 mm spherical cores are set at each of the three combustion chamber ignition positions.

2.3 Grid-independence and validation of computational models

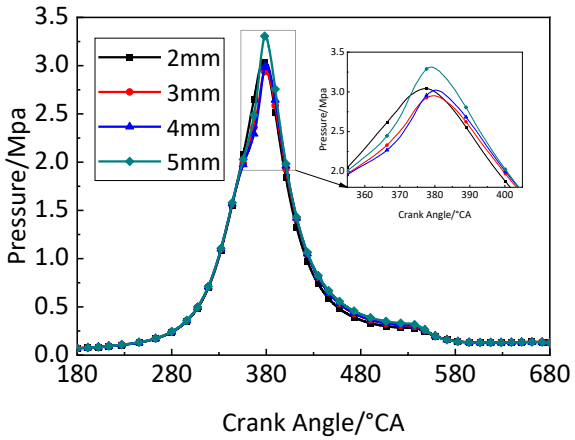

Fig. 2. In-cylinder mean pressure under different grid sizes

In the grid-independent verification, four basic grid sizes of combustion chambers are set up with 2, 3, 4 and 5 mm grids. The settings of adaptive grid encryption are opened. Meanwhile, the velocity, temperature and component of the calculated basin are encrypted with the maximum refinement level of 3. The variation of the in-cylinder mean pressure curve crank angle for different combustion chamber grid sizes is given in Fig. 2. With the improvement of grid accuracy, the difference between the calculated results of grids within 5 mm becomes

smaller and smaller, which can indicate that the grid independence is verified. In order to save computational cost and maintain high computational accuracy, the basic grid size of 3 mm with adaptive encryption is used in the numerical simulation.

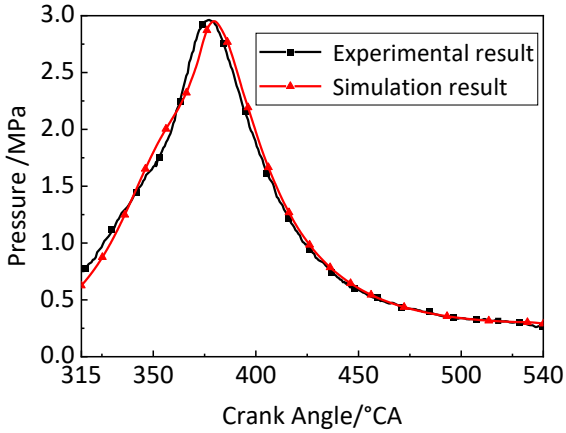

Fig. 3. Model validation for in-cylinder mean pressure

In order to verify the accuracy of the CFD model, the same working conditions as those in literature [5] are set for simulation. The parameters of the working conditions in Table 2 are used to simulate the XRE without PHG. The comparison results of the in-cylinder mean pressure are shown in Fig. 3. The maximum error between the experimental results and the simulation results is less than 10%, and the error of the peak pressure is less than 2%. Concurrently, the in-cylinder pressure trend obtained from the simulation is consistent with the experimental results. It is allowed in the simulation of engine [14], so the calculation of PHG can be carried out.

3. SIMULATION RESULTS AND DISCUSSION

3.1 In-cylinder flow analysis

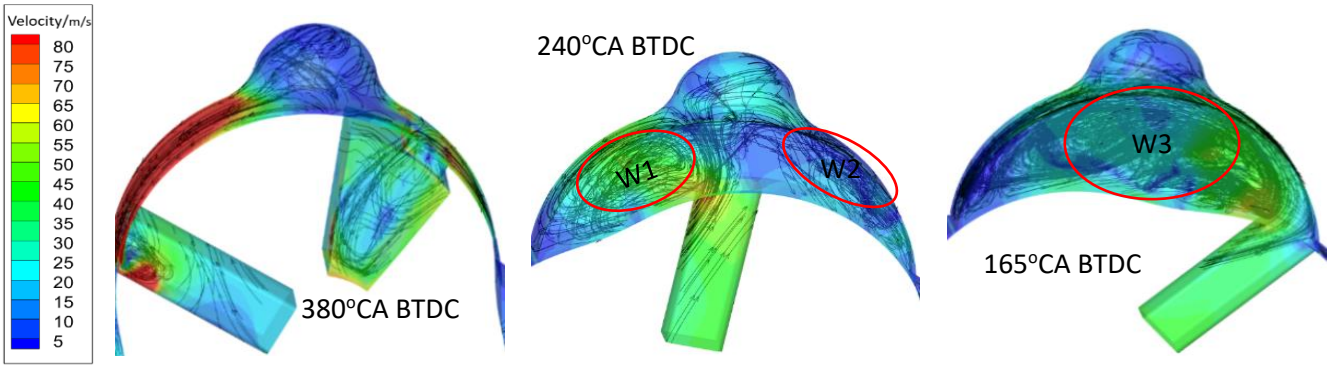

（1） Intake start （2） Intake middle （3） Intake end

Fig .4. Distribution of in-cylinder velocity field and streamline under different crank angle

Fig . 4 shows the distribution of the flow and velocity fields from the beginning to middle and then to end of intake stage. At the initial moment, the intake airflow flows into the combustion chamber through the slit on the left side of the chamber. In this time the intake and exhaust processes exist simultaneously. At the middle of the intake, the intake airflow hits the left side of the combustion chamber to form a large vortex W1, and the remaining airflow forms a smaller, opposite direction vortex W2 on the right side of the chamber. At the end of the intake, the airflow enters along the outer side of the chamber to form a large vortex W3 inside, and the streamlines are more uniformly distributed. From the in-cylinder intake process of the XRE, it can be seen that the airflow forms a strong vortex mass as it enters the combustion chamber. These vortices contribute to the rapid mixing of fuel and air during the operation of the engine, and then form a more homogeneous mixture.

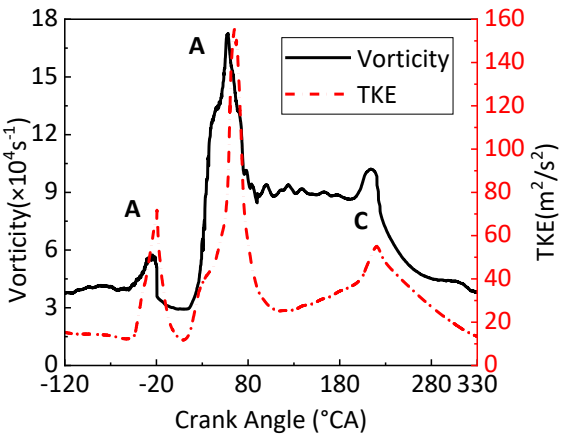

Fig . 5. Variation of in-cylinder mean TKE and vorticity curve crank angle

The in-cylinder TKE and vorticity can reflect the change of in-cylinder flow field, which is the key factor affecting flame propagation [15]. From Fig. 5, it can be seen that the change trend of in-cylinder mean TKE is the same as vorticity with the increase of crank angle. In general, it shows an increasing trend followed by a

decreasing trend. There are three peak values A, B and C, which are respectively located at the beginning, the middle and the end of the intake stage. Peak B is the largest with two smaller peaks A and C on the left and right. The main reason for the appearance of peak A is that the high-speed airflow enters the slit of combustion chamber from the intake port at the beginning of the intake stage. The slit is small and more blocked, resulting in high velocity, large airflow disturbance here, and a small increase in mean TKE and vorticity. The second peak B is located in the middle of the intake stage, at this time the combustion chamber formed two large vortexes W1 and W2. The gas in the combustion chamber flows violently and disturbs rapidly, so the mean TKE and vorticity rise rapidly to the maximum. Then the vortices W1 and W2 gradually break up and melt into a larger but reduced intensity vortex W3, so the mean TKE and vorticity begin to decrease. The third peak C is at the end of the intake stage, at this time the vortex W3 starts to dissipate and disappear. So the mean TKE and vorticity increase to a certain extent and then decrease. Therefore, vortex A and vortex B are important factors affecting in-cylinder flow and mixture formation.

In addition, it is found that after PHG, the in-cylinder mean TKE and vorticity don't change much except for a small range rise at the peak during the intake and compression process. The main reason is that PHG reduces the gas flow density and increases the gas flow rate. Further, this can enhance the diffusion effect of airflow and the change of airflow direction, resulting in increased airflow disturbance in the combustion chamber. As a result, the TKE and vorticity also increase.

3.2 Effect of PHG on combustion process

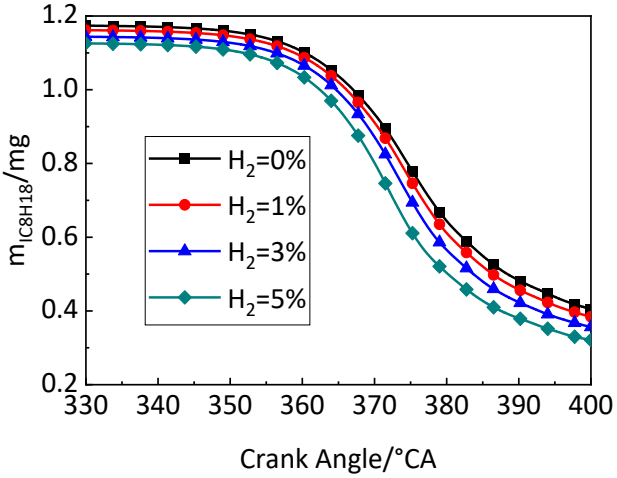

(1) IC8H18（gasoline）

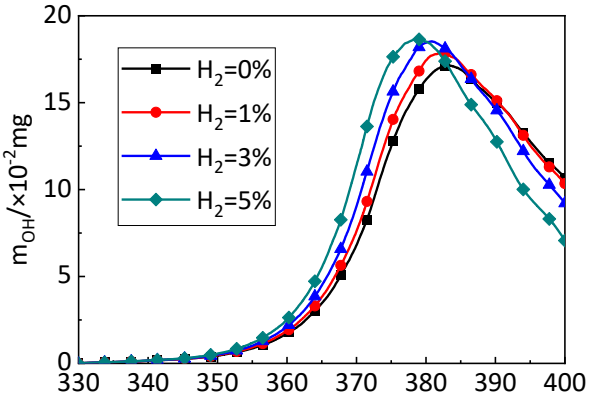

(2) OH

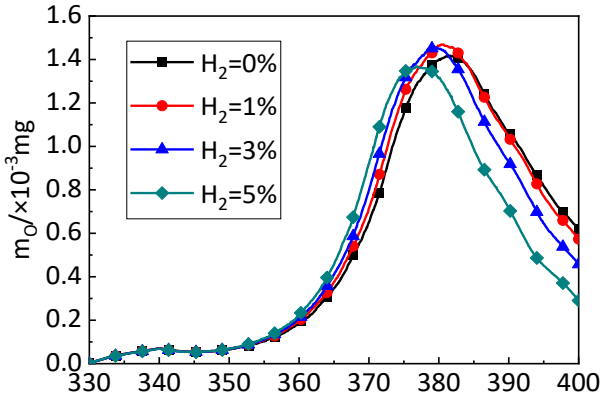

(3) O

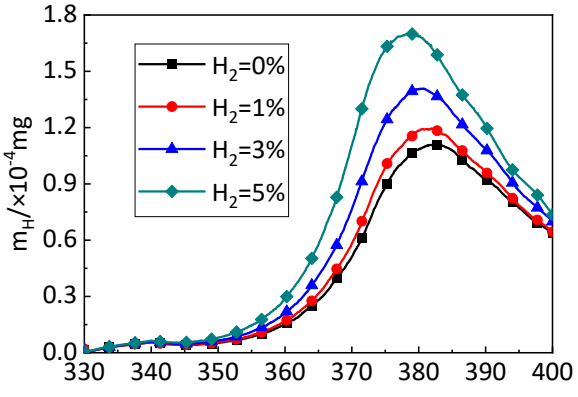

(4) H

Fig. 6. Mass of IC8H18 (1)、OH (2)、O (3)and H (4) radicals versus crank angle under different EFHB

The variation curves of the masses of IC8H18 (1), OH radical (2), O radical (3) and H radical (4) versus crank angle for different EFHB are given in Fig 6. It can be seen that in the initial stage of combustion (30°AC BTDC to 10°AC BTDC), there is little difference in the mass fraction of OH, H and O radicals. And the change of gasoline is not obvious. This is mainly because ignition energy is the same and the spark plug ignites the same area of

combustible mixture during the process. After 10°AC BTDC, there is a significant increase of OH and H radicals with the increase of EFHB. Meanwhile, the crank angle corresponding to the peak mass of these radicals is advanced and the gasoline consumption rate becomes faster. This is because PHG can accelerate the reaction rate of $OH+H_2 \Leftrightarrow H_2O+H$ and generate more H radicals, which in turn promotes the reaction rate of $H+O_2 \Leftrightarrow OH+O$ [16]. As important branched reactions in gasoline combustion process, these two reactions promote each other and directly determine the burning rate of the fuel. All in all, PHG can increase the mass of OH, O and H radicals and effectively shorten the formation process of fire nuclei. What's more, it has an accelerating effect on the burning rate of fuel and can increase the rate of gasoline consumption. Namely, PHG is beneficial to the improvement of fuel utilization rate of XRE.

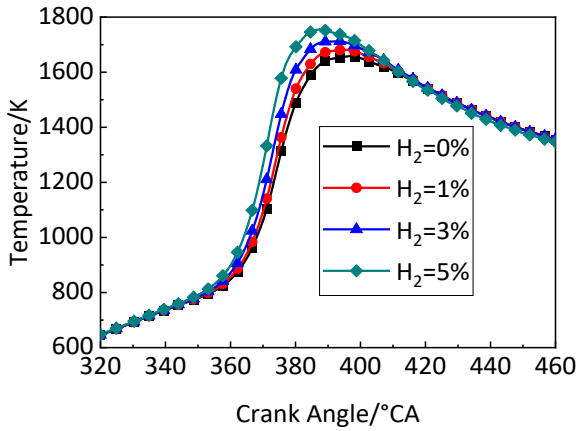

Fig. 7. In-cylinder mean temperature versus crank angle under different EFHB

In order to compare the difference of in-cylinder combustion between PHG and pure gasoline, the variation curves of in-cylinder mean temperature versus crank angle under different EFHB are presented in Fig. 7. It is found that PHG can significantly increase mean temperature of the combustion chamber. Meanwhile, the crank angle corresponding to the peak temperature is advanced. As the EFHB increases, the peak temperature also increases. When the EFHB is 5%, the peak temperature in the combustion chamber is increased by 6.4% compared with pure gasoline.

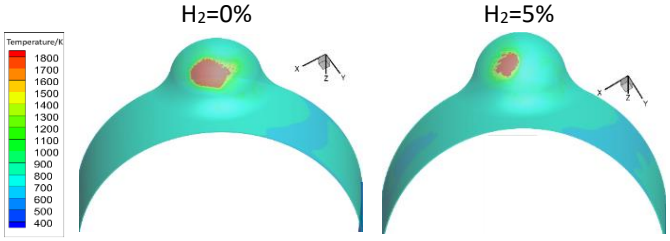

5°CA ATDC

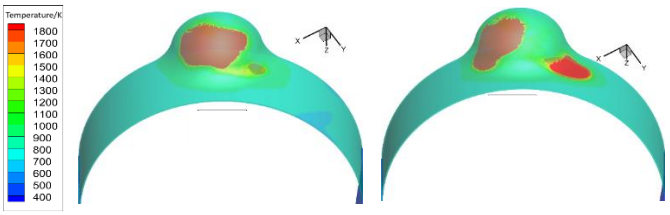

10°CA ATDC

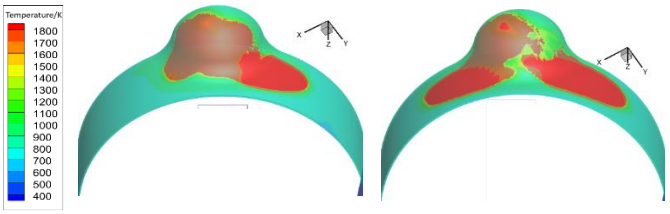

15°CA ATDC

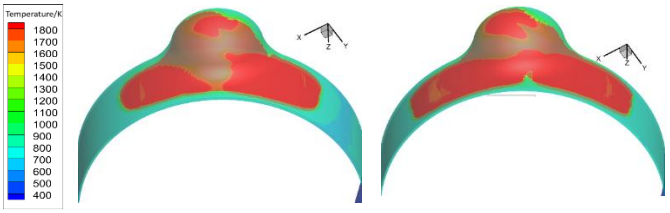

20°CA ATDC

Fig. 8. Cloud map of in-cylinder temperature change

Fig. 8 displays the comparison of the in-cylinder temperature clouds for pure gasoline and PHG at 5% EFHB for four moments. At 5°CA ATDC, the difference between the two temperature clouds is not significant. The combustion area of pure gasoline is located in the middle of the spherical combustion chamber while that of PHG is on the left side of the combustion chamber. At 10°CA ATDC, the difference between the two temperature clouds begins to appear. The combustion area of pure gasoline continues to expand in the middle of the chamber. The combustion area of PHG not only expands on the left side of the combustion chamber, but also on the right side of the chamber. At 15°CA ATDC, the combustion area of pure gasoline spreads to the right side of the chamber. By comparison, the combustion area of PHG expands on the left and right sides respectively. At 20°CA ATDC, the temperature cloud distribution of both tends to be the same. But the combustion area of PHG is larger than that of pure gasoline. Moreover, the flame center temperature is higher than that of pure gasoline.

From the above, it can be seen that the combustion of HB mixture on the left and right sides of the combustion chamber is obviously better than that of pure gasoline. Namely, the flame propagation speed to the left and right sides of the combustion chamber is obviously greater than that of pure gasoline. These indicate that blending a small amount of hydrogen can make the flame propagate farther and improve the combustion of fuel on the left and right sides of the

combustion chamber. Besides, the PHG can make the combustion area more uniform and help solve the problem of incomplete combustion in the slit on both sides.

4. CONCLUSIONS

In this paper, a 3D numerical simulation model of an XRE with PHG is established, and the engine flow filed and combustion performances are studied under different EFHB. The following conclusions are obtained:

(1) Two vortexes in opposite directions are generated on both sides of the combustion chamber in the intake stage. They interact with each other and promote the mixing process of gas components, leading to the maximum of in-cylinder mean TKE and vorticity.

(2) In respect to the combustion performance of XRE, the PHG can increase the content of OH, H and O radicals, and promote the generation of radicals, leading to the acceleration of the consumption rate of gasoline. The mixing of hydrogen in XRE could accelerate the combustion speed, and widen the flame to both sides of the combustion chamber, and present a more uniform combustion area.

ACKNOWLEDGEMENT

Thanks for the support from the Science and Technology on Plasma Dynamics Laboratory Program (No.6142202210201) and The Green Aerotechnics Research Institute of Chongqing Jiaotong University.

REFERENCE

[1] Shkolnik A, Littera D, Nickerson M, et al. Development of a small rotary SI/CI combustion engine[C]. SAE Technical Paper, 2014.

[2] Yang J, Ji C, Wang S, et al. Numerical investigation on the mixture formation and combustion processes of a gasoline rotary engine with direct injected hydrogen enrichment [J]. Applied Energy, 2018, 224: 34-41.

[3] Amrouche F, Erickson P, Park J. Extending the lean operation limit of a gasoline Wankel rotary engine using hydrogen enrichment[J]. International Journal of Hydrogen Energy. 2016, 41(32):14261-14271.

[4] Nickerson M, Kopache A, Shkolnik A, et al. Preliminary development of a 30 kW heavy fueled compression ignition rotary X engine with target 45% brake thermal efficiency[C]. SAE Technical Paper, 2018.

[5] Costa T, Nickerson M, Littera D, Martins J, et al. Measurement and prediction of heat transfer losses on the XMv3 rotary engine[J]. SAE Int. J. Engines, 2016, 9(4):2368-2380.

[6] Littera D, Nickerson M, Kopache A, et al. Development of the XMv3 high efficiency cycloidal engine[C]. SAE Technical Paper, 2015.

[7] Leboeuf M, Dufault J, Nickerson M, et al. Performance of a low-blowby sealing system for a high efficiency rotary engine[C]. SAE Technical Paper, 2018.

[8] Wang S, Ji C, Zhang B, et al. Effect of CO2 dilution on combustion and emissions characteristics of the hydrogen-enriched gasoline engine[J]. Energy, 2016, 96:118-126.

[9] Ji C, Cong X, Wang S, et al. Performance of a hydrogen-blended gasoline direct injection engine under various second gasoline direct injection timings[J]. Energy Conversion and Management, 2018, 171:1704-1711.

[10] Fan B, Zhang Y, Pan J, et al. The influence of hydrogen injection strategy on mixture formation and combustion process in a port injection rotary engine fueled with natural gas/hydrogen blends[J]. Energy Conversion and Management, 2018, 173:527-538.

[11] Fan B, Pan J, Liu Y, et al. Numerical investigation of mixture formation and combustion in a hydrogen direct injection plus natural gas port injection rotary engine[J]. International Journal of Hydrogen Energy, 2018, 43:4632-4644.

[12] Yang J, Ji C, Wang S, et al. Numerical investigation of the effects of hydrogen enrichment on combustion and emissions formation processes in a gasoline rotary engine [J]. Energy Conversion and Management, 2017, 151: 136-146.

[13] Liu Y, Jia M, Xie M, et al. Enhancement on a skeletal kinetic model for primary reference fuel oxidation by using a semidecoupling methodology[J]. Energy & Fuels, 2012, 26:7069-7083.

[14] Yang J, Ji C, Wang S, et al. A comparative study of mixture formation and combustion processes in a gasoline Wankel rotary engine with hydrogen port and direct injection enrichment [J]. Energy conversion and management, 2018, 168: 21-31.

[15] Su T, Ji C, Wang S, et al. Investigation on combustion and emissions characteristics of a hydrogen-blended n-butanol rotary engine [J]. International Journal of Hydrogen Energy, 2017, 42(41): 26142-26151.

[16] Ji C, Su T, Wang S, et al. Effect of hydrogen addition on combustion and emissions performance of a gasoline rotary engine at part load and stoichiometric conditions[J]. Energy conversion and management, 2016, 121: 272-280.